

A precision measurement of the $D_{s1}(2536)^+$ meson mass and decay width

The *BABAR* Collaboration

July 9, 2018

Abstract

The decay width and the mass of the $D_{s1}(2536)^\pm$ have been measured via the decay channel $D_{s1}^\pm \rightarrow D^{*\pm} K_S^0$ using 232 fb^{-1} of data collected with the *BABAR* detector at the PEP-II asymmetric-energy e^+e^- storage ring. The result for the decay width is $\Gamma(D_{s1}^\pm) = (1.03 \pm 0.05 \pm 0.12) \text{ MeV}/c^2$, with the first error denoting the statistical uncertainty and the second one the systematic uncertainty. For the mass, a value of $m(D_{s1}^\pm) = (2534.85 \pm 0.02 \pm 0.40) \text{ MeV}/c^2$ has been obtained. The systematic error is dominated by the uncertainty on the $D^{*\pm}$ mass. The mass difference between the D_{s1}^\pm and $D^{*\pm}$ has been measured to be $\Delta m = (524.85 \pm 0.02 \pm 0.04) \text{ MeV}/c^2$.

Submitted to the 33rd International Conference on High-Energy Physics, ICHEP 06,
26 July—2 August 2006, Moscow, Russia.

Stanford Linear Accelerator Center, Stanford University, Stanford, CA 94309

Work supported in part by Department of Energy contract DE-AC03-76SF00515.

The BABAR Collaboration,

B. Aubert, R. Barate, M. Bona, D. Boutigny, F. Couderc, Y. Karyotakis, J. P. Lees, V. Poireau,
V. Tisserand, A. Zghiche

*Laboratoire de Physique des Particules, IN2P3/CNRS et Université de Savoie, F-74941 Annecy-Le-Vieux,
France*

E. Grauges

Universitat de Barcelona, Facultat de Física, Departament ECM, E-08028 Barcelona, Spain

A. Palano

Università di Bari, Dipartimento di Fisica and INFN, I-70126 Bari, Italy

J. C. Chen, N. D. Qi, G. Rong, P. Wang, Y. S. Zhu

Institute of High Energy Physics, Beijing 100039, China

G. Eigen, I. Ofte, B. Stugu

University of Bergen, Institute of Physics, N-5007 Bergen, Norway

G. S. Abrams, M. Battaglia, D. N. Brown, J. Button-Shafer, R. N. Cahn, E. Charles, M. S. Gill,
Y. Groyzman, R. G. Jacobsen, J. A. Kadyk, L. T. Kerth, Yu. G. Kolomensky, G. Kukartsev, G. Lynch,
L. M. Mir, T. J. Orimoto, M. Pripstein, N. A. Roe, M. T. Ronan, W. A. Wenzel

Lawrence Berkeley National Laboratory and University of California, Berkeley, California 94720, USA

P. del Amo Sanchez, M. Barrett, K. E. Ford, A. J. Hart, T. J. Harrison, C. M. Hawkes, S. E. Morgan,
A. T. Watson

University of Birmingham, Birmingham, B15 2TT, United Kingdom

T. Held, H. Koch, B. Lewandowski, M. Pelizaeus, K. Peters, T. Schroeder, M. Steinke
Ruhr Universität Bochum, Institut für Experimentalphysik 1, D-44780 Bochum, Germany

J. T. Boyd, J. P. Burke, W. N. Cottingham, D. Walker

University of Bristol, Bristol BS8 1TL, United Kingdom

D. J. Asgeirsson, T. Cuhadar-Donszelmann, B. G. Fulsom, C. Hearty, N. S. Knecht, T. S. Mattison,
J. A. McKenna

University of British Columbia, Vancouver, British Columbia, Canada V6T 1Z1

A. Khan, P. Kyberd, M. Saleem, D. J. Sherwood, L. Teodorescu

Brunel University, Uxbridge, Middlesex UB8 3PH, United Kingdom

V. E. Blinov, A. D. Bukin, V. P. Druzhinin, V. B. Golubev, A. P. Onuchin, S. I. Serednyakov,
Yu. I. Skovpen, E. P. Solodov, K. Yu Todyshev

Budker Institute of Nuclear Physics, Novosibirsk 630090, Russia

D. S. Best, M. Bondioli, M. Bruinsma, M. Chao, S. Curry, I. Eschrich, D. Kirkby, A. J. Lankford, P. Lund,
M. Mandelkern, R. K. Mommsen, W. Roethel, D. P. Stoker

University of California at Irvine, Irvine, California 92697, USA

S. Abachi, C. Buchanan

University of California at Los Angeles, Los Angeles, California 90024, USA

S. D. Foulkes, J. W. Gary, O. Long, B. C. Shen, K. Wang, L. Zhang
University of California at Riverside, Riverside, California 92521, USA

H. K. Hadavand, E. J. Hill, H. P. Paar, S. Rahatlou, V. Sharma
University of California at San Diego, La Jolla, California 92093, USA

J. W. Berryhill, C. Campagnari, A. Cunha, B. Dahmes, T. M. Hong, D. Kovalskyi, J. D. Richman
University of California at Santa Barbara, Santa Barbara, California 93106, USA

T. W. Beck, A. M. Eisner, C. J. Flacco, C. A. Heusch, J. Kroseberg, W. S. Lockman, G. Nesom, T. Schalk,
B. A. Schumm, A. Seiden, P. Spradlin, D. C. Williams, M. G. Wilson
University of California at Santa Cruz, Institute for Particle Physics, Santa Cruz, California 95064, USA

J. Albert, E. Chen, A. Dvoretzkii, F. Fang, D. G. Hitlin, I. Narsky, T. Piatenko, F. C. Porter, A. Ryd,
A. Samuel
California Institute of Technology, Pasadena, California 91125, USA

G. Mancinelli, B. T. Meadows, K. Mishra, M. D. Sokoloff
University of Cincinnati, Cincinnati, Ohio 45221, USA

F. Blanc, P. C. Bloom, S. Chen, W. T. Ford, J. F. Hirschauer, A. Kreisel, M. Nagel, U. Nauenberg,
A. Olivas, W. O. Ruddick, J. G. Smith, K. A. Ulmer, S. R. Wagner, J. Zhang
University of Colorado, Boulder, Colorado 80309, USA

A. Chen, E. A. Eckhart, A. Soffer, W. H. Toki, R. J. Wilson, F. Winklmeier, Q. Zeng
Colorado State University, Fort Collins, Colorado 80523, USA

D. D. Altenburg, E. Feltresi, A. Hauke, H. Jasper, J. Merkel, A. Petzold, B. Spaan
Universität Dortmund, Institut für Physik, D-44221 Dortmund, Germany

T. Brandt, V. Klose, H. M. Lacker, W. F. Mader, R. Nogowski, J. Schubert, K. R. Schubert, R. Schwierz,
J. E. Sundermann, A. Volk
Technische Universität Dresden, Institut für Kern- und Teilchenphysik, D-01062 Dresden, Germany

D. Bernard, G. R. Bonneaud, E. Latour, Ch. Thiebaux, M. Verderi
Laboratoire Leprince-Ringuet, CNRS/IN2P3, Ecole Polytechnique, F-91128 Palaiseau, France

P. J. Clark, W. Gradl, F. Muheim, S. Playfer, A. I. Robertson, Y. Xie
University of Edinburgh, Edinburgh EH9 3JZ, United Kingdom

M. Andreotti, D. Bettoni, C. Bozzi, R. Calabrese, G. Cibinetto, E. Luppi, M. Negrini, A. Petrella,
L. Piemontese, E. Prencipe
Università di Ferrara, Dipartimento di Fisica and INFN, I-44100 Ferrara, Italy

F. Anulli, R. Baldini-Ferroli, A. Calcaterra, R. de Sangro, G. Finocchiaro, S. Pacetti, P. Patteri,
I. M. Peruzzi,¹ M. Piccolo, M. Rama, A. Zallo
Laboratori Nazionali di Frascati dell'INFN, I-00044 Frascati, Italy

¹Also with Università di Perugia, Dipartimento di Fisica, Perugia, Italy

A. Buzzo, R. Capra, R. Contri, M. Lo Vetere, M. M. Macri, M. R. Monge, S. Passaggio, C. Patrignani,
E. Robutti, A. Santroni, S. Tosi

Università di Genova, Dipartimento di Fisica and INFN, I-16146 Genova, Italy

G. Brandenburg, K. S. Chaisanguanthum, M. Morii, J. Wu

Harvard University, Cambridge, Massachusetts 02138, USA

R. S. Dubitzky, J. Marks, S. Schenk, U. Uwer

Universität Heidelberg, Physikalisches Institut, Philosophenweg 12, D-69120 Heidelberg, Germany

D. J. Bard, W. Bhimji, D. A. Bowerman, P. D. Dauncey, U. Egede, R. L. Flack, J. A. Nash,
M. B. Nikolich, W. Panduro Vazquez

Imperial College London, London, SW7 2AZ, United Kingdom

P. K. Behera, X. Chai, M. J. Charles, U. Mallik, N. T. Meyer, V. Ziegler

University of Iowa, Iowa City, Iowa 52242, USA

J. Cochran, H. B. Crawley, L. Dong, V. Eyges, W. T. Meyer, S. Prell, E. I. Rosenberg, A. E. Rubin

Iowa State University, Ames, Iowa 50011-3160, USA

A. V. Gritsan

Johns Hopkins University, Baltimore, Maryland 21218, USA

A. G. Denig, M. Fritsch, G. Schott

Universität Karlsruhe, Institut für Experimentelle Kernphysik, D-76021 Karlsruhe, Germany

N. Arnaud, M. Davier, G. Grosdidier, A. Höcker, F. Le Diberder, V. Lepeltier, A. M. Lutz, A. Oyanguren,
S. Pruvot, S. Rodier, P. Roudeau, M. H. Schune, A. Stocchi, W. F. Wang, G. Wormser

*Laboratoire de l'Accélérateur Linéaire, IN2P3/CNRS et Université Paris-Sud 11, Centre Scientifique
d'Orsay, B.P. 34, F-91898 ORSAY Cedex, France*

C. H. Cheng, D. J. Lange, D. M. Wright

Lawrence Livermore National Laboratory, Livermore, California 94550, USA

C. A. Chavez, I. J. Forster, J. R. Fry, E. Gabathuler, R. Gamet, K. A. George, D. E. Hutchcroft,
D. J. Payne, K. C. Schofield, C. Touramanis

University of Liverpool, Liverpool L69 7ZE, United Kingdom

A. J. Bevan, F. Di Lodovico, W. Menges, R. Sacco

Queen Mary, University of London, E1 4NS, United Kingdom

G. Cowan, H. U. Flaecher, D. A. Hopkins, P. S. Jackson, T. R. McMahon, S. Ricciardi, F. Salvatore,
A. C. Wren

*University of London, Royal Holloway and Bedford New College, Egham, Surrey TW20 0EX, United
Kingdom*

D. N. Brown, C. L. Davis

University of Louisville, Louisville, Kentucky 40292, USA

J. Allison, N. R. Barlow, R. J. Barlow, Y. M. Chia, C. L. Edgar, G. D. Lafferty, M. T. Naisbit,
J. C. Williams, J. I. Yi

University of Manchester, Manchester M13 9PL, United Kingdom

C. Chen, W. D. Hulsbergen, A. Jawahery, C. K. Lae, D. A. Roberts, G. Simi

University of Maryland, College Park, Maryland 20742, USA

G. Blaylock, C. Dallapiccola, S. S. Hertzbach, X. Li, T. B. Moore, S. Saremi, H. Staengle

University of Massachusetts, Amherst, Massachusetts 01003, USA

R. Cowan, G. Sciolla, S. J. Sekula, M. Spitznagel, F. Taylor, R. K. Yamamoto

*Massachusetts Institute of Technology, Laboratory for Nuclear Science, Cambridge, Massachusetts 02139,
USA*

H. Kim, S. E. McLachlin, P. M. Patel, S. H. Robertson

McGill University, Montréal, Québec, Canada H3A 2T8

A. Lazzaro, V. Lombardo, F. Palombo

Università di Milano, Dipartimento di Fisica and INFN, I-20133 Milano, Italy

J. M. Bauer, L. Cremaldi, V. Eschenburg, R. Godang, R. Kroeger, D. A. Sanders, D. J. Summers,
H. W. Zhao

University of Mississippi, University, Mississippi 38677, USA

S. Brunet, D. Côté, M. Simard, P. Taras, F. B. Viaud

Université de Montréal, Physique des Particules, Montréal, Québec, Canada H3C 3J7

H. Nicholson

Mount Holyoke College, South Hadley, Massachusetts 01075, USA

N. Cavallo,² G. De Nardo, F. Fabozzi,³ C. Gatto, L. Lista, D. Monorchio, P. Paolucci, D. Piccolo,
C. Sciacca

Università di Napoli Federico II, Dipartimento di Scienze Fisiche and INFN, I-80126, Napoli, Italy

M. A. Baak, G. Raven, H. L. Snoek

*NIKHEF, National Institute for Nuclear Physics and High Energy Physics, NL-1009 DB Amsterdam, The
Netherlands*

C. P. Jessop, J. M. LoSecco

University of Notre Dame, Notre Dame, Indiana 46556, USA

T. Allmendinger, G. Benelli, L. A. Corwin, K. K. Gan, K. Honscheid, D. Hufnagel, P. D. Jackson,
H. Kagan, R. Kass, A. M. Rahimi, J. J. Regensburger, R. Ter-Antonyan, Q. K. Wong

Ohio State University, Columbus, Ohio 43210, USA

N. L. Blount, J. Brau, R. Frey, O. Igonkina, J. A. Kolb, M. Lu, R. Rahmat, N. B. Sinev, D. Strom,
J. Strube, E. Torrence

University of Oregon, Eugene, Oregon 97403, USA

²Also with Università della Basilicata, Potenza, Italy

³Also with Università della Basilicata, Potenza, Italy

A. Gaz, M. Margoni, M. Morandin, A. Pompili, M. Posocco, M. Rotondo, F. Simonetto, R. Stroili, C. Voci
Università di Padova, Dipartimento di Fisica and INFN, I-35131 Padova, Italy

M. Benayoun, H. Briand, J. Chauveau, P. David, L. Del Buono, Ch. de la Vaissière, O. Hamon,
B. L. Hartfiel, M. J. J. John, Ph. Leruste, J. Malcès, J. Ocariz, L. Roos, G. Therin
*Laboratoire de Physique Nucléaire et de Hautes Energies, IN2P3/CNRS, Université Pierre et Marie
Curie-Paris6, Université Denis Diderot-Paris7, F-75252 Paris, France*

L. Gladney, J. Panetta
University of Pennsylvania, Philadelphia, Pennsylvania 19104, USA

M. Biasini, R. Covarelli
Università di Perugia, Dipartimento di Fisica and INFN, I-06100 Perugia, Italy

C. Angelini, G. Batignani, S. Bettarini, F. Bucci, G. Calderini, M. Carpinelli, R. Cenci, F. Forti,
M. A. Giorgi, A. Lusiani, G. Marchiori, M. A. Mazur, M. Morganti, N. Neri, E. Paoloni, G. Rizzo,
J. J. Walsh
Università di Pisa, Dipartimento di Fisica, Scuola Normale Superiore and INFN, I-56127 Pisa, Italy

M. Haire, D. Judd, D. E. Wagoner
Prairie View A&M University, Prairie View, Texas 77446, USA

J. Biesiada, N. Danielson, P. Elmer, Y. P. Lau, C. Lu, J. Olsen, A. J. S. Smith, A. V. Telnov
Princeton University, Princeton, New Jersey 08544, USA

F. Bellini, G. Cavoto, A. D'Orazio, D. del Re, E. Di Marco, R. Faccini, F. Ferrarotto, F. Ferroni,
M. Gaspero, L. Li Gioi, M. A. Mazzoni, S. Morganti, G. Piredda, F. Polci, F. Safai Tehrani, C. Voena
Università di Roma La Sapienza, Dipartimento di Fisica and INFN, I-00185 Roma, Italy

M. Ebert, H. Schröder, R. Waldi
Universität Rostock, D-18051 Rostock, Germany

T. Adye, N. De Groot, B. Franek, E. O. Olaiya, F. F. Wilson
Rutherford Appleton Laboratory, Chilton, Didcot, Oxon, OX11 0QX, United Kingdom

R. Aleksan, S. Emery, A. Gaidot, S. F. Ganzhur, G. Hamel de Monchenault, W. Kozanecki, M. Legendre,
G. Vasseur, Ch. Yèche, M. Zito
DSM/Daphnia, CEA/Saclay, F-91191 Gif-sur-Yvette, France

X. R. Chen, H. Liu, W. Park, M. V. Purohit, J. R. Wilson
University of South Carolina, Columbia, South Carolina 29208, USA

M. T. Allen, D. Aston, R. Bartoldus, P. Bechtle, N. Berger, R. Claus, J. P. Coleman, M. R. Convery,
M. Cristinziani, J. C. Dingfelder, J. Dorfan, G. P. Dubois-Felsmann, D. Dujmic, W. Dunwoodie,
R. C. Field, T. Glanzman, S. J. Gowdy, M. T. Graham, P. Grenier,⁴ V. Halyo, C. Hast, T. Hryn'ova,
W. R. Innes, M. H. Kelsey, P. Kim, D. W. G. S. Leith, S. Li, S. Luitz, V. Luth, H. L. Lynch,
D. B. MacFarlane, H. Marsiske, R. Messner, D. R. Muller, C. P. O'Grady, V. E. Ozcan, A. Perazzo,
M. Perl, T. Pulliam, B. N. Ratcliff, A. Roodman, A. A. Salnikov, R. H. Schindler, J. Schwiening,
A. Snyder, J. Stelzer, D. Su, M. K. Sullivan, K. Suzuki, S. K. Swain, J. M. Thompson, J. Va'vra, N. van

⁴Also at Laboratoire de Physique Corpusculaire, Clermont-Ferrand, France

Bakel, M. Weaver, A. J. R. Weinstein, W. J. Wisniewski, M. Wittgen, D. H. Wright, A. K. Yarritu, K. Yi,
C. C. Young

Stanford Linear Accelerator Center, Stanford, California 94309, USA

P. R. Burchat, A. J. Edwards, S. A. Majewski, B. A. Petersen, C. Roat, L. Wilden

Stanford University, Stanford, California 94305-4060, USA

S. Ahmed, M. S. Alam, R. Bula, J. A. Ernst, V. Jain, B. Pan, M. A. Saeed, F. R. Wappler, S. B. Zain

State University of New York, Albany, New York 12222, USA

W. Bugg, M. Krishnamurthy, S. M. Spanier

University of Tennessee, Knoxville, Tennessee 37996, USA

R. Eckmann, J. L. Ritchie, A. Satpathy, C. J. Schilling, R. F. Schwitters

University of Texas at Austin, Austin, Texas 78712, USA

J. M. Izen, X. C. Lou, S. Ye

University of Texas at Dallas, Richardson, Texas 75083, USA

F. Bianchi, F. Gallo, D. Gamba

Università di Torino, Dipartimento di Fisica Sperimentale and INFN, I-10125 Torino, Italy

M. Bomben, L. Bosisio, C. Cartaro, F. Cossutti, G. Della Ricca, S. Dittongo, L. Lanceri, L. Vitale

Università di Trieste, Dipartimento di Fisica and INFN, I-34127 Trieste, Italy

V. Azzolini, N. Lopez-March, F. Martinez-Vidal

IFIC, Universitat de Valencia-CSIC, E-46071 Valencia, Spain

Sw. Banerjee, B. Bhuyan, C. M. Brown, D. Fortin, K. Hamano, R. Kowalewski, I. M. Nugent, J. M. Roney,
R. J. Sobie

University of Victoria, Victoria, British Columbia, Canada V8W 3P6

J. J. Back, P. F. Harrison, T. E. Latham, G. B. Mohanty, M. Pappagallo

Department of Physics, University of Warwick, Coventry CV4 7AL, United Kingdom

H. R. Band, X. Chen, B. Cheng, S. Dasu, M. Datta, K. T. Flood, J. J. Hollar, P. E. Kutter, B. Mellado,
A. Mihalyi, Y. Pan, M. Pierini, R. Prepost, S. L. Wu, Z. Yu

University of Wisconsin, Madison, Wisconsin 53706, USA

H. Neal

Yale University, New Haven, Connecticut 06511, USA

1 INTRODUCTION

The discovery of the mesons $D_{sJ}^*(2317)^+$ and $D_{sJ}(2460)^+$ [1, 2], with masses considerably lower than predicted by potential models [3, 4], has renewed experimental and theoretical interest in the spectroscopy of charmed mesons. For a complete understanding of the charmed strange meson spectrum, a comprehensive knowledge of the parameters of all known D_s^+ mesons is mandatory. In this analysis, a precision measurement of the mass and the decay width of the meson $D_{s1}(2536)^+$ has been performed. The mass is currently reported by the PDG with a precision of $0.6 \text{ MeV}/c^2$, while only an upper limit of $2.3 \text{ MeV}/c^2$ is given for the decay width [5]. These values are based on measurements with 20 times fewer reconstructed D_{s1}^+ candidates compared to this analysis. The *BABAR* experiment, in addition to its excellent tracking and vertexing capabilities, provides a rich source of charmed hadrons, enabling an analysis of the D_{s1}^+ with high statistics and small errors.

Since the uncertainty of the D^{*+} mass is large ($0.4 \text{ MeV}/c^2$ [5]), we perform a measurement of the mass difference defined by

$$\Delta m(D_{s1}^+) = m(D_{s1}^+) - m(D^{*+}) - m(K_S^0). \quad (1)$$

Additionally, due to the correlation between the masses, the D_{s1}^+ signal in the mass difference spectrum is much more narrow than the one from the D_{s1}^+ mass spectrum alone.

2 THE *BABAR* DETECTOR AND DATASET

The data sample used in this analysis corresponds to 232 fb^{-1} collected with the *BABAR* detector at the PEP-II storage ring from e^+e^- collisions at or just below the $\Upsilon(4S)$ resonance. Furthermore, 1.16 million D_{s1}^+ Monte Carlo events were generated for each of the two decay modes which are used for the determination of the detector resolution model. Finally, for resolution studies, D^0 and K_S^0 samples were analyzed using 5% of the main data sample and 20 million simulated $e^+e^- \rightarrow c\bar{c}$ generic Monte Carlo continuum events.

The *BABAR* detector is described elsewhere [6] in detail. Charged particles are detected with a combination of a five-layer double-sided silicon vertex tracker (SVT) and a 40-layer drift chamber (DCH) filled with a mixture of helium and isobutane, both embedded in the 1.5 T solenoidal magnetic field. The transverse momentum resolution is approximately $\sigma_{p_t}/p_t = 0.0013(p_t/\text{GeV}/c) \oplus 0.0045$. Charged particle identification is done via energy loss measurement within the SVT and DCH, and via the Cherenkov light detected in a ring imaging Cherenkov detector (DIRC). Photons are detected with a CsI(Tl) electromagnetic calorimeter consisting of 6580 CsI(Tl) crystals. The instrumented flux return (IFR) contains resistive plate chambers for the identification of muons and long-lived neutral hadrons. For the event simulation we use the Monte Carlo generator EVTGEN [7] with a full detector simulation that uses GEANT4 [8].

The most critical aspect of this analysis is the quality of the track reconstruction. The track-finding algorithm is based on tracks found by the trigger system and by standalone track reconstruction in the SVT and DCH. The parameters of a given track are determined using a Kalman filter algorithm [9], which makes optimal use of the hit information and corrects for energy loss and multiple scattering in the material traversed and for inhomogeneities in the magnetic field. The material-traversal corrections change the track momentum according to the expected average energy loss and increase the covariance for track parameters to account for both multiple scattering and the variance in the energy loss. The latter depends on the particle velocity, so each track fit is

performed separately for five particle hypotheses: electron, muon, pion, kaon and proton. A simplified model of the *BABAR* detector material distribution is used in the Kalman filter algorithm; a wrong simulation of the material will result in a wrong energy loss correction in the reconstruction. Besides a good description of the tracking region, a detailed knowledge of the magnetic field is also essential for a precise track reconstruction. The solenoid field itself has been well measured. The field strength in the tracking volume is known to an accuracy of 0.2 mT. More uncertain is the contribution of the solenoid field to the magnetization of the permanent magnets used for final focusing and bending of the beams. This is discussed in more detail in section 4.3.

3 ANALYSIS METHOD

3.1 D_{s1}^+ candidate reconstruction

Two decay modes are reconstructed: in both modes the D_{s1}^+ decays to $D^{*+}K_s^0$, with the K_s^0 decaying into $\pi^+\pi^-$ and the D^{*+} into $D^0\pi^+$. The D^0 decays either into $K^-\pi^+$ or $K^-\pi^+\pi^-\pi^-$. In the following, we refer to these two decay modes as $K4\pi$ and $K6\pi$, respectively, where also the charge conjugated states are included.

For the D^0 candidate reconstruction, charged kaon and pion candidates are combined to form $K^-\pi^+$ ($K^-\pi^+\pi^+\pi^-$) final states. Fits to the D^0 mass spectra yield a mean value of 1863.6 MeV/ c^2 and a signal resolution of 7.4 MeV/ c^2 (8.1 MeV/ c^2) for the $K4\pi$ ($K6\pi$) decay mode. The signal region is chosen as a mass window of ± 18 MeV/ c^2 (± 14 MeV/ c^2) centered around the obtained mean value. The D^0 candidates are each combined with an additional charged pion to form D^{*+} candidates. The fits to the D^{*+} - D^0 mass difference yield a mean value of 145.4 MeV/ c^2 and a signal resolution of 0.19 MeV/ c^2 (0.24 MeV/ c^2) for $K4\pi$ ($K6\pi$). The signal region is chosen as a mass window of ± 1.5 MeV/ c^2 centered around the derived mean value for both decay modes. Finally, K_s^0 candidates are created from oppositely charged tracks. From the fits to the K_s^0 mass distributions one obtains a mean value of 497.2 MeV/ c^2 and a resolution of 2.5 MeV/ c^2 for both decay modes. For the further analysis we define the K_s^0 signal region as a ± 10 MeV/ c^2 mass window centered around the signal mean value for both modes.

The background of the K_s^0 spectrum is further reduced by restricting the angle between the K_s^0 direction of flight and the line connecting the primary vertex and the K_s^0 vertex to values smaller than 0.15 rad. The D^{*+} candidates are finally combined with the K_s^0 candidates to form D_{s1}^+ candidates. In order to suppress combinatorial background, a momentum $p^* > 2.7$ GeV/ c in the center of mass system (CMS) is required for D_{s1}^+ candidates. In addition, this restricts the source of the D_{s1}^+ candidates to $e^+e^- \rightarrow c\bar{c}$ continuum production. A kinematic fit is applied to the D_{s1}^+ candidates which satisfy the above selection criteria in such a way, that the tracks for each composed particle have the same origin. The position of the D_{s1}^+ vertex is required to be consistent with the e^+e^- interaction region. Since the mass difference $\Delta m(D_{s1}^+)$ is measured, no mass constraint is applied. The probability of the vertex fit is required to be greater than 0.1%. Initially, more than one D_{s1}^+ candidate per event is reconstructed. Although the multiple use of tracks within one reconstructed decay tree is excluded, there might be multiple D_{s1}^+ candidates sharing the same daughter candidate. After applying all selection criteria, the average multiplicity of D_{s1}^+ candidates per event is 1.008 and 1.02 for the two decay modes. The selection efficiency is 16% for the $K4\pi$ decay mode and 11% for the $K6\pi$ mode.

The resulting mass difference spectra $\Delta m(D_{s1}^+)$ for MC and data are shown in Section 3.3 and 3.4, respectively. A double Gaussian is fitted to the data spectrum as a rough estimate of the

width of the signal. The results for the total width, calculated by adding the weighted Gaussian widths in quadrature, are $1.55 \pm 0.15 \text{ MeV}/c^2$ and $1.66 \pm 0.26 \text{ MeV}/c^2$ for mode $K4\pi$ and $K6\pi$, respectively. Note that for this preliminary fit the intrinsic width and the resolution have not been taken separately into account.

3.2 Resolution model

Although very clean signals with more than 2400 (2900) entries have been obtained for decay mode $K4\pi$ ($K6\pi$), it is not feasible to obtain the resolution model and the intrinsic width from a single fit to data with all parameters allowed to vary. Instead a resolution model is derived from the corresponding D_{s1}^+ Monte Carlo samples. The generation of $e^+e^- \rightarrow c\bar{c}$ fragmentation events with high accuracy is a difficult task, so deviations between simulated and real data are possible. In particular the distribution of the CMS momentum p^* of the reconstructed D_{s1}^+ mesons differs between data and Monte Carlo events. In order to extract a reliable resolution model from Monte Carlo, the model is determined as a function of p^* . Another method to compensate for the inaccuracies of the simulation is to weight the Monte Carlo spectrum according to the p^* distribution obtained from data and extract the resolution model from the weighted Monte Carlo sample. Since the second method relies on both real data and Monte Carlo data and is sensitive to the chosen p^* binning, it is used as a systematic check and the resolution model is derived from the first method.

The resolution can be extracted by calculating the difference of the invariant mass of a reconstructed candidate and the corresponding generated mass. The derived distribution consists only of the deconvolved resolution part of the D_{s1}^+ signal. Since for the measurement of the D_{s1}^+ mass the mass difference $\Delta m(D_{s1}^+)$ is taken, the mass difference $\Delta m_g(D_{s1}^+)$ of the corresponding generated candidates has to be subtracted to obtain the deconvolved distribution:

$$\Delta m_{res} = \Delta m(D_{s1}^+) - \Delta m_g(D_{s1}^+). \quad (2)$$

The procedure is the same for both decay modes. The Monte Carlo sample is divided into 25 p^* bins with a width of $0.07 \text{ GeV}/c$ in the range from $2.70 \text{ GeV}/c$ to $4.45 \text{ GeV}/c$. An unbinned maximum likelihood fit of Δm_{res} is performed for each bin of p^* using a probability density function (PDF) assembled from Gaussian functions with fit parameters $\Delta m_{res,0}$, r and σ_0 :

$$R(\Delta m_{res}) = \int_{\sigma_0}^{r\sigma_0} \frac{1}{r\sigma^2} e^{-\frac{(\Delta m_{res} - \Delta m_{res,0})^2}{2\sigma^2}} d\sigma, \quad (3)$$

where $\Delta m_{res,0}$ is the mean value and the width is integrated from a minimum value of σ_0 up to a maximum of $r\sigma_0$. The scale parameter for the upper width limit r is determined for each p^* bin, but does not vary drastically with p^* . Fixed values for r are obtained from a fit with a constant function to the r distribution which yields $r = 5.64 \pm 0.05$ (6.40 ± 0.06) for decay mode $K4\pi$ ($K6\pi$). A non-constant 1st order polynomial can be fitted to the r distribution for mode $K4\pi$; this scenario is investigated in Section 4.2. The fits to Δm_{res} are repeated with r fixed to the constant value obtained which leaves σ_0 as the only free parameter for the width. For each p^* bin, σ_0 is recalculated. The new σ_0 distribution can be best parameterized by the second order polynomial below with coefficients b_i .

$$\sigma_0(p^*) = b_0 + b_1 p^* + b_2 p^{*2}. \quad (4)$$

3.3 Validation of the resolution model

To verify that the resolution model is reliable, we applied it to the $\Delta m(D_{s1}^+)$ distribution of the D_{s1}^+ Monte Carlo data sample

$$\Delta m(D_{s1}^+) = S(\Delta\mu(D_{s1}^+), \Gamma(D_{s1}^+)) * R(\Delta m_{res}). \quad (5)$$

The generated D_{s1}^+ mass difference distribution $S(\Delta\mu(D_{s1}^+), \Gamma(D_{s1}^+))$ in the simulation follows a non-relativistic Breit-Wigner distribution with mean value $\Delta\mu(D_{s1}^+)$ and width $\Gamma(D_{s1}^+)$ (Table 1). The fit of this Breit-Wigner convoluted with the resolution function to Monte Carlo data must return the generated values for the mass difference $\Delta\mu(D_{s1}^+)$ and the decay width $\Gamma(D_{s1}^+)$. Since the convolution of the resolution model and the Breit-Wigner function cannot be handled analytically one has to use numerical integration methods instead. To compute the convolution integral the *Trapezoid Sum Rule* method has been applied. The convolution window has been chosen as $\pm 10 \text{ MeV}/c^2$, which is about 10 times the width of the resolution function, and was divided into 200 bins. The applied method returns stable fit results for reconstructed Monte Carlo and reproduces the input values for the mass difference and width in the simulation with sufficient accuracy (Fig. 1, Table 1). The differences between the reconstructed values and the generated values are assigned as systematic uncertainties, which are $-7 \text{ keV}/c^2$ ($-14 \text{ keV}/c^2$) for the mass difference and $-2 \text{ keV}/c^2$ ($-9 \text{ keV}/c^2$) for the width.

Table 1: Results of the test fits to the MC data (statistical errors only) for both decay modes, compared with the generated values.

Parameter	$K4\pi$	$K6\pi$	generated
$\Delta\mu(D_{s1}^+) / \text{MeV}/c^2$	27.737 ± 0.003	27.730 ± 0.003	27.744
$\Gamma(D_{s1}^+) / \text{MeV}/c^2$	0.998 ± 0.005	0.991 ± 0.007	1.000

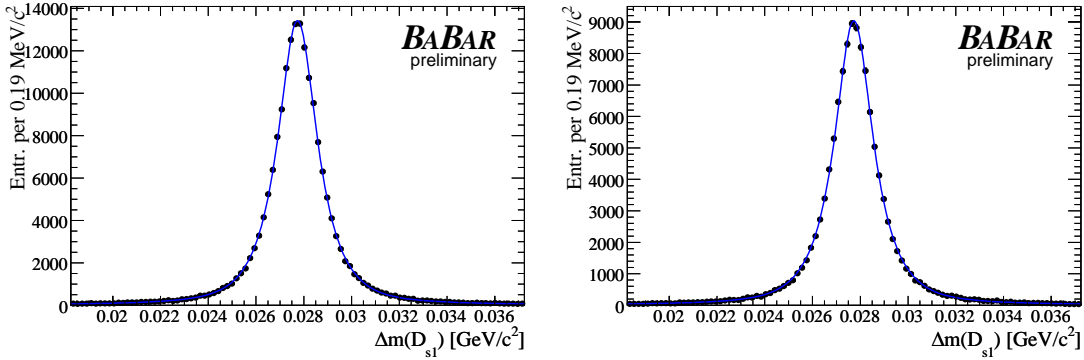


Figure 1: Fit of the convolution of the non-relativistic Breit-Wigner function and the resolution function to the $\Delta m(D_{s1}^+)$ distribution in MC (dots) as a crosscheck for the p^* -dependent resolution model. Left: decay mode $K4\pi$; right: decay mode $K6\pi$

3.4 Fit to the data

The assumption that the D_{s1}^+ lineshape $S(\Delta\mu(D_{s1}^+), \Gamma(D_{s1}^+))$ follows a non-relativistic Breit-Wigner, as used for the MC, is not sufficient for the measurement of the intrinsic width. A better and commonly used description of a resonance lineshape is the following, *relativistic* Breit-Wigner function:

$$BW(m) \propto \frac{mm_0\Gamma}{(m^2 - m_0^2)^2 + m_0^2\Gamma^2} \quad (6)$$

To measure the mass difference $\Delta\mu(D_{s1}^+)$ and the intrinsic width $\Gamma(D_{s1}^+)$, the extracted p^* -dependent resolution model $R(\Delta m_{res})$ is convoluted with the relativistic Breit-Wigner distribution and then fitted to data using an unbinned maximum likelihood fit. For the convolution the same numerical integration method as described for the MC test fit (Section 3.3) is applied. The background is described by a linear function. The fit parameters obtained for both decay modes are listed in table 2. The corresponding mass distributions are shown with the fits in Fig. 2.

Table 2: Results of the fit to the data (statistical errors only) for both decay modes.

Parameter	$K4\pi$	$K6\pi$
$\Delta\mu(D_{s1}^+) / \text{MeV}/c^2$	27.209 ± 0.028	27.180 ± 0.023
$\Gamma(D_{s1}^+) / \text{MeV}/c^2$	1.112 ± 0.068	0.990 ± 0.059
Signal yield (events)	2401 ± 47	2959 ± 51

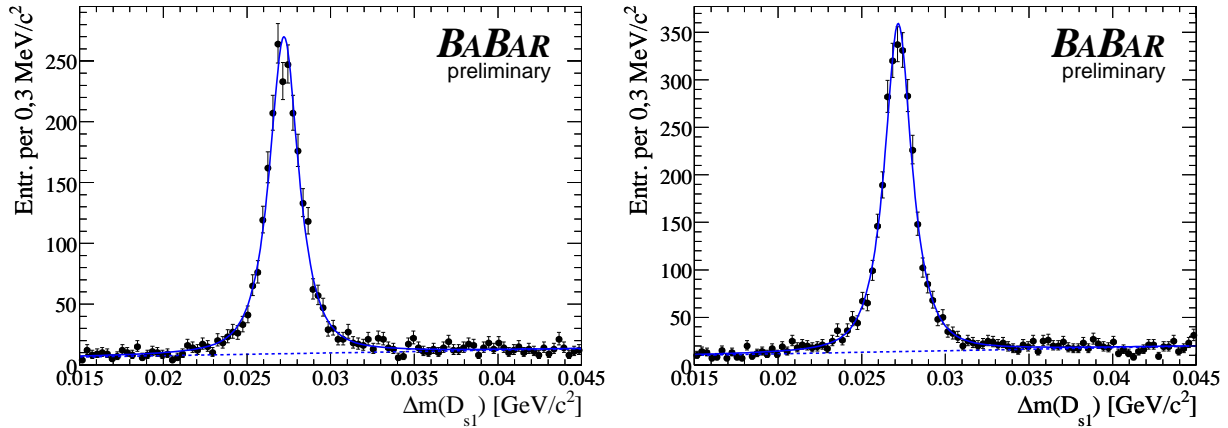


Figure 2: Fit to the data (dots) of the relativistic Breit-Wigner function convoluted with the p^* -dependent resolution function to the $\Delta m(D_{s1}^+)$ spectrum to obtain the mass difference $\Delta\mu(D_{s1}^+)$ and width $\Gamma(D_{s1}^+)$. The background is described by a first order polynomial, shown by the dotted line. Left: decay mode $K4\pi$; right: decay mode $K6\pi$.

4 SYSTEMATIC UNCERTAINTIES

Sources of systematic uncertainties can be divided into three categories: a) discrepancies between the resolution in data and Monte Carlo (Section 4.1); b) extraction of the resolution model and the fit procedure (Section 4.2); c) uncertainties due to inaccuracies in the track reconstruction (Section 4.3). The results for the different systematic errors are listed in Table 3.

4.1 Resolution studies

A D^0 sample including both decays $D^0 \rightarrow K^- \pi^+$ and $D^0 \rightarrow K^- \pi^+ \pi^+ \pi^-$ and a $K_S^0 \rightarrow \pi^+ \pi^-$ sample have been extracted from data and generic $c\bar{c}$ Monte Carlo and are used for resolution studies. The D^0 and K_S^0 mesons have been reconstructed in the same way as described in Section 3.1, but without a requirement for the origin of the particles. Due to the negligible width of these two mesons, the resolution can be directly obtained from a fit to the respective signals. To avoid momentum-related discrepancies, the samples are divided into p^* -dependent subsets. The resolution function from Eq. 3 is fitted to each data and $c\bar{c}$ Monte Carlo subset. The full width at half maximum (FWHM) is calculated for each bin as a measure of the width of the resolution function. For the ratio between the MC and the data resolution, values of 0.90 ± 0.01 for the D^0 as well as for the K_S^0 samples are obtained by fitting a constant function to the p^* -dependent ratio. In order to measure the impact of this deviation on the results for the D_{s1}^+ signal lineshape in data, the width of the resolution function obtained in Section 3.2 is enlarged by 10%. The additional resolution is assumed to follow a Gaussian distribution. To achieve this widening, the Δm_{res} spectrum (divided into p^* bins as used for the standard fit explained in Section 3.2) is smeared by a Gaussian distribution with a certain width σ_e which yields a spectrum with a FWHM 10% larger than the original one. The parameters of the resolution function are obtained as described in Section 3.2. With this resolution function, the fit to data is repeated. As expected, the mass is not affected while the width is lowered by $67 \text{ keV}/c^2$ (mode $K4\pi$) and $52 \text{ keV}/c^2$ (mode $K6\pi$).

4.2 Fit procedure

Systematic uncertainties concerning the applied method to extract the D_{s1}^+ mass and width have been studied.

Resolution model As described in Section 3.3, the resolution model has been tested on the MC data sample. The small differences between the reconstructed values for $\Delta\mu(D_{s1}^+)$ and $\Gamma(D_{s1}^+)$ and the respective generated ones are assigned as systematic errors.

In a first check, the parameter r of the resolution function is alternatively parameterized by a 1^{st} order polynomial. With r now depending on p^* rather than being constant, the parameter σ_0 is estimated as described in Section 3.2. Using the new resolution model, one obtains a negligible shift of the mass and $-25 \text{ keV}/c^2$ ($+7 \text{ keV}/c^2$) for the decay width.

Another check involves varying the parameter r within one standard deviation δr of its statistical error. Parameterizing σ_0 using the modified r value, the fit to data is repeated with these resolution parameters. As a conservative estimate the larger value of the relative change observed for $r - \delta r$ and $r + \delta r$ is taken as an uncertainty. The mass is not affected while the width changes by $-9 \text{ keV}/c^2$ ($K4\pi$) and $-27 \text{ keV}/c^2$ ($K6\pi$).

Numerical integration for convolution Lowering and enlarging the integration range by $\pm 1 \text{ MeV}/c^2$ while keeping the bin width constant does not yield significant changes. Doubling and halving the bin size while using the standard $20 \text{ MeV}/c^2$ integration interval yields no relative change of $\Delta\mu(D_{s1}^+)$ and $\Gamma(D_{s1})$ either, compared with the standard values.

Background parameterization In the fit to the $\Delta m(D_{s1}^+)$ distribution for data the combinatorial background was parameterized using a first order polynomial. As a systematic check, the latter is replaced by a second order polynomial which yields a mass shift of $-3 \text{ keV}/c^2 (< 0.5 \text{ keV}/c^2)$ and a modification to the width by $-7 \text{ keV}/c^2 (-27 \text{ keV}/c^2)$. In a second test, the background was parameterized by a power-law distribution, e.g. using $BG(\Delta m(D_{s1}^+)) = a_0 + a_1 \Delta m(D_{s1}^+) + a_2 \Delta m(D_{s1}^+)^{a_3}$. Both the mass difference and the width do not noticeably change, compared with the standard values. Thus, the deviations from the fit with the 2^{nd} order polynomial are taken as the systematic uncertainty arising from the background parameterization.

Mass window Enlarging the boundaries of the fitted $\Delta m(D_{s1}^+)$ standard region ($0.015 - 0.045 \text{ MeV}/c^2$) by $10 \text{ MeV}/c^2$ has no significant impact on the $\Delta\mu(D_{s1}^+)$ value and changes the width slightly by $+4 \text{ keV}/c^2 (-13 \text{ keV}/c^2)$.

p^* correction Two strategies - the parameterization and the weighting method - have been followed to take the observed discrepancy between the p^* distributions for data and MC data into account. The results obtained from both approaches are consistent within their statistical errors, giving confidence in the results obtained from the parameterization method. The deviation between the two methods can be assigned as the systematic uncertainty arising from the applied correction method, whereby only the width is noticeably affected by $-21 \text{ keV}/c^2 (-9 \text{ keV}/c^2)$.

4.3 Detector conditions

In the third category of systematic uncertainties, sources arising from charged particle track reconstruction have been studied. The amount of material located inside the inner tracking volume (SVT and DCH) as well as the understanding of the B field inside that volume plays an important role for the reconstruction of charged particles. In addition to this, a dependency of the reconstructed mass difference on the p^* momentum and on the azimuthal and polar angles θ and ϕ of the D_{s1}^+ has been studied.

Material inside tracking volume It is possible that the amount of material traversed by charged particles in the tracking volume is underestimated [10]. This would result in an incorrect energy loss correction for the tracks. Two scenarios have been investigated. First, it is assumed that the amount of material inside the total volume (SVT and DCH) is underestimated by 10%. Second, it is assumed that only the amount of SVT material is underestimated, by 20%. To study the effect, the density of the material at the corresponding detector component is increased by the respective number. With the new detector conditions, the data are reanalyzed and the fit to data is repeated using the standard resolution model with the parameters obtained in Section 3.2. As a conservative estimate, the largest deviations of the mass and width obtained from these fits are taken as the systematic uncertainty arising from the tracking region material modification. The results are shown in Table 3.

Magnetic Field The main component of the magnetic field, which is an essential component for the momentum measurement, is the solenoid field which is itself well measured. More uncertain is the contribution of the solenoid field to the magnetization of the permanent magnets used for final focusing and bending of the beams. The magnitude of the solenoid B field is changed by $\pm 0.02\%$ for the systematic study. The magnetization is varied by $\pm 20\%$ in order to account for differences between the direct field measurements and the permeability measurements. The largest deviations observed for the rescaled solenoid field and the rescaled magnetization are added in quadrature and used as a conservative estimate of the systematic uncertainty arising from the B field.

Length scale Another source of uncertainty for the momentum arises from the distance scale. The position of the wires in the DCH is known with a precision of $40\ \mu\text{m}$. With a drift chamber radius of $\approx 40\ \text{cm}$, this yields a relative precision of 0.01% . As an estimate for the uncertainty of the momentum due to the length scale, a systematic error half the size of the uncertainty obtained from the $\pm 0.02\%$ variation of the solenoid field is assigned. For the mass difference, this yields a shift of $-5\ \text{keV}/c^2$ ($-8\ \text{keV}/c^2$) for mode $K4\pi$ ($K6\pi$). The width is shifted by $+1\ \text{keV}/c^2$ ($+6\ \text{keV}/c^2$).

SVT alignment Detector misalignment can affect the measurement of the angles between the tracks and possibly the track momenta. This effect has not yet been studied in this analysis. As a conservative estimate, the results obtained from SVT misalignment studies performed for the Λ_c mass measurement [10] will be used as a systematic uncertainty for the D_{s1}^+ mass. This yields an additional error of $\pm 23\ \text{keV}/c^2$.

Track quality For the standard D_{s1}^+ candidate selection as described in Section 3.1, no lower limit has been set for the number of drift chamber hits left by a charged particle. To estimate the effect of improved track quality, the selection of the D_{s1}^+ candidates has been repeated, requiring that only those π and K candidates are used for the D_{s1}^+ reconstruction which have left at least 20 hits in the drift chamber. The determination of the resolution model has been repeated using the new data samples. The mass difference is shifted by $+5\ \text{keV}/c^2$ ($-14\ \text{keV}/c^2$), while the width is shifted by $-105\ \text{keV}/c^2$ ($-92\ \text{keV}/c^2$) with respect to the standard values obtained in Section 3.4. In a second test, the π originating from the D^{*+} decay has been excluded from the tighter track selection. Because of its small transverse momentum, it will not traverse large parts of the drift chamber. The mass difference is shifted by $-8\ \text{keV}/c^2$ ($< 0.5\ \text{keV}/c^2$), while the width is shifted by $-110\ \text{keV}/c^2$ ($-57\ \text{keV}/c^2$). As a conservative estimate, the deviations obtained from the first measurement will be used as a systematic uncertainty.

Charge dependence The mass difference $\Delta\mu(D_{s1}^+)$ and the width $\Gamma(D_{s1}^+)$ have been determined separately for both charges of the D_{s1} . The values obtained are consistent within errors with the results for the complete data sample (Table 4). Comparing the different values obtained with the respective standard values yields for the mass difference a χ^2 of 1.31 (0.34) for mode $K4\pi$ ($K6\pi$) and for the width a χ^2 of 2.08 (0.85).

Momentum dependence The mass difference and the width is measured for five different p^* bins in the range between 2.7 and $4.7\ \text{GeV}/c$. The results obtained do not vary drastically compared with the standard mass difference value obtained from the complete data sample. The weighted mean values for the mass difference and the width lie within the error range of the respective values for the full data sample (Table 4). Comparing the p^* distributions with the respective standard

values yields for the mass difference a χ^2 of 0.76 (3.09) for mode $K4\pi$ ($K6\pi$) and for the width a χ^2 of 3.11 (0.36).

Angular dependence A dependency of the reconstructed mass on the azimuthal angle ϕ has been observed using the high statistic D^0 data sample created for the resolution studies, while no such effect is visible in the corresponding $c\bar{c}$ MC. The ϕ dependency of the reconstructed D^0 mass follows a sine wave and averages to zero when running over the complete data and thus over the whole ϕ range. Furthermore, the mass difference $\Delta\mu(D_{s1}^+)$ and the width $\Gamma(D_{s1}^+)$ have been measured in bins of the angle θ of the D_{s1}^+ and in bins of the azimuthal angle ϕ . In both cases, the values obtained for the different bins are consistent with the values obtained from the fits to the complete data sample. The weighted mean values all lie within the error range of the standard values for $\Delta\mu(D_{s1}^+)$ and $\Gamma(D_{s1}^+)$, respectively (Table 4). Comparing the θ distributions with the respective standard values yields for the mass difference a χ^2 of 5.54 (0.97) for mode $K4\pi$ ($K6\pi$) and for the width a χ^2 of 0.98 (6.76). For the ϕ distributions one obtains for the mass difference a χ^2 of 5.41 (2.87) and for the width a χ^2 of 3.28 (0.37). Larger χ^2 values are due to bins with greater deviations, caused by the small number of D_{s1}^+ candidates available in this range.

Run dependence Finally, the mass difference and the width have been determined separately for different data taking periods. The results obtained for $\Delta\mu(D_{s1}^+)$ and $\Gamma(D_{s1}^+)$ lie within the error range of the standard values for the mass difference and the width, respectively (Table 4). Comparing the different values obtained with the respective standard values yields for the mass difference a χ^2 of 0.55 (3.36) for mode $K4\pi$ ($K6\pi$) and for the width a χ^2 of 1.16 (0.39).

In summary, for both the mass difference $\Delta\mu(D_{s1}^+)$ and the decay width $\Gamma(D_{s1}^+)$, no significant dependency on the D_{s1}^+ momentum, charge and angle or on the time of data-taking have been observed. The fits to the different data subsamples return values within the error range of the results obtained from the fits to the complete data sample.

4.4 Techniques for combining results

The results obtained for the two decay modes are combined using an expanded χ^2 method that allows different correlations between the individual components of the systematic uncertainties. As a crosscheck, the results are combined using a Best Linear Unbiased Estimate (BLUE) technique [11] which takes correlated and uncorrelated errors separately into account. The results obtained from the methods are consistent with each other. Since the BLUE method delivers only one single combined error, the results from the first method are reported.

5 SUMMARY

We have presented a high precision measurement of the mass and the decay width of the meson $D_{s1}(2536)^+$ using the decay mode $D_{s1}^+ \rightarrow D^{*+} K_S^0$. The mass difference between D_{s1}^+ and $D^{*+} K_S^0$ for the two reconstructed decay modes is measured to be

$$\begin{aligned}\Delta\mu(D_{s1}^+)_{K4\pi} &= 27.209 \pm 0.028 \pm 0.031 \text{ MeV}/c^2, \\ \Delta\mu(D_{s1}^+)_{K6\pi} &= 27.180 \pm 0.023 \pm 0.043 \text{ MeV}/c^2,\end{aligned}$$

Table 3: Summary of systematic uncertainties.

	$\Delta\mu(D_{s1}^+) / \text{keV}/c^2$		$\Gamma(D_{s1}^+) / \text{keV}/c^2$	
	$K4\pi$	$K6\pi$	$K4\pi$	$K6\pi$
Resolution width +10%	± 1	< 0.5	± 67	± 52
MC validation	± 7	± 14	± 2	± 9
Parameterization of r	< 0.5	< 0.5	± 25	± 7
Variation of r	< 0.5	< 0.5	± 9	± 27
Numerical integration (width)	< 0.5	< 0.5	< 0.5	< 0.5
Numerical integration (steps)	< 0.5	< 0.5	< 0.5	< 0.5
Background parameterization	± 3	< 0.5	± 7	± 27
Mass window	± 1	< 0.5	± 4	± 13
p^* correction	< 0.5	± 1	± 21	± 9
Detector material	± 14	± 24	± 20	± 29
B field	± 10	± 16	± 7	± 13
Length scale	± 5	± 8	± 1	± 6
SVT alignment	± 23	± 23	-	-
Track quality	± 5	± 14	± 105	± 92
Quadratic sum	± 31	± 43	± 131	± 119

 Table 4: Measurements of $\Delta\mu(D_{s1}^+)$ and $\Gamma(D_{s1}^+)$ in dependence of several variables. The first row shows the results from the fits to the full data sample, followed by the charge dependent measurements. Lines 4 to 6 list the weighted mean values obtained from p^* , θ and ϕ depending measurements. The last two rows contain the results for different data taking periods.

Dependency	$\Delta\mu(D_{s1}^+) / \text{MeV}/c^2$		$\Gamma(D_{s1}^+) / \text{MeV}/c^2$	
	$K4\pi$	$K6\pi$	$K4\pi$	$K6\pi$
Full data	27.209 ± 0.028	27.180 ± 0.023	1.112 ± 0.068	0.990 ± 0.059
D_{s1}^+	27.176 ± 0.041	27.193 ± 0.033	1.201 ± 0.101	1.042 ± 0.086
D_{s1}^-	27.239 ± 0.037	27.166 ± 0.033	1.007 ± 0.092	0.933 ± 0.082
$p^*(D_{s1}^+)$	27.196 ± 0.073	27.204 ± 0.058	1.222 ± 0.188	0.932 ± 0.155
$\theta(D_{s1}^+)$	27.211 ± 0.053	27.181 ± 0.045	1.107 ± 0.129	0.996 ± 0.116
$\phi(D_{s1}^+)$	27.206 ± 0.062	27.179 ± 0.053	1.108 ± 0.151	0.992 ± 0.133
<i>Run1</i> + 2	27.236 ± 0.041	27.232 ± 0.036	1.022 ± 0.098	0.947 ± 0.092
<i>Run3</i> + 4	27.188 ± 0.039	27.145 ± 0.031	1.167 ± 0.098	0.958 ± 0.078

with the first error denoting the statistical uncertainty and the second one the systematic uncertainty. These results correspond to a relative error of 0.15% for the mass difference. This lies within the range of precision achievable with the *BABAR* detector: the J/ψ mass has been reconstructed with a relative error of 0.05% [6].

Combining the results, while taking the systematic errors including the uncertainties of the D^{*+} mass ($\pm 0.4 \text{ MeV}/c^2$) and of the K_S^0 mass ($\pm 0.022 \text{ MeV}/c^2$) into account, yields a final value for the D_{s1}^+ mass of

$$m(D_{s1}^+) = 2534.85 \pm 0.02 \pm 0.40 \text{ MeV}/c^2,$$

while the PDG value for the mass is given as $2535.35 \pm 0.34 \pm 0.50 \text{ MeV}/c^2$. The error on the measured D_{s1}^+ mass is dominated by the uncertainty of the D^{*+} mass. The mass difference between the D_{s1}^+ and the D^{*+} follows from these results as

$$\Delta m = m(D_{s1}^+) - m(D^{*+}) = 524.85 \pm 0.02 \pm 0.04 \text{ MeV}/c^2.$$

The decay width is measured to be

$$\begin{aligned} \Gamma(D_{s1}^+)_{K4\pi} &= 1.112 \pm 0.068 \pm 0.131 \text{ MeV}/c^2, \\ \Gamma(D_{s1}^+)_{K6\pi} &= 0.990 \pm 0.059 \pm 0.119 \text{ MeV}/c^2. \end{aligned}$$

The final combined value for decay width is

$$\Gamma(D_{s1}^+) = 1.03 \pm 0.05 \pm 0.12 \text{ MeV}/c^2.$$

The result for the mass difference $\Delta m = m(D_{s1}^+) - m(D^{*+})$ represents an improvement in precision by a factor of 14 compared with the current PDG value of $525.3 \pm 0.6 \pm 0.1 \text{ MeV}/c^2$. Our result deviates by 1σ from the larger PDG value. The precision achieved is comparable with other recent high precision analyses performed at *BABAR* like the Λ_c mass measurement ($m(\Lambda_c) = 2286.46 \pm 0.04 \pm 0.14 \text{ MeV}/c^2$) [10]. Furthermore, this analysis presents for the first time a direct measurement of the D_{s1}^+ decay width with small errors rather than just an upper limit, which is currently stated by the PDG as $2.3 \text{ MeV}/c^2$.

6 ACKNOWLEDGMENTS

We are grateful for the extraordinary contributions of our PEP-II colleagues in achieving the excellent luminosity and machine conditions that have made this work possible. The success of this project also relies critically on the expertise and dedication of the computing organizations that support *BABAR*. The collaborating institutions wish to thank SLAC for its support and the kind hospitality extended to them. This work is supported by the US Department of Energy and National Science Foundation, the Natural Sciences and Engineering Research Council (Canada), Institute of High Energy Physics (China), the Commissariat à l’Energie Atomique and Institut National de Physique Nucléaire et de Physique des Particules (France), the Bundesministerium für Bildung und Forschung and Deutsche Forschungsgemeinschaft (Germany), the Istituto Nazionale di Fisica Nucleare (Italy), the Foundation for Fundamental Research on Matter (The Netherlands), the Research Council of Norway, the Ministry of Science and Technology of the Russian Federation, and the Particle Physics and Astronomy Research Council (United Kingdom). Individuals have received support from the Marie-Curie IEF program (European Union) and the A. P. Sloan Foundation.

References

- [1] The *BABAR* Collaboration, B. Aubert *et al.*, Phys. Rev. Lett. **90**, 242001 (2003).
- [2] The CLEO Collaboration, D. Besson *et al.*, Phys. Rev. D **68**, 032002 (2003).
- [3] S. Godfrey and N. Isgur, Phys. Rev. D **32**, 189 (1985).
- [4] M. Di Pierro and E. Eichten, Phys. Rev. D **64**, 114004 (2001).
- [5] Particle Data Group, S. Eidelmann *et al.*, Phys. Lett. B **592**, 1 (2004).
- [6] The *BABAR* Collaboration, B. Aubert *et al.*, Nucl. Instrum. Meth. A **479**, 1 (2002).
- [7] D. J. Lange, Nucl. Instrum. Meth. A **462**, 152 (2001).
- [8] The GEANT4 Collaboration, S. Agostinelli *et al.*, Nucl. Instrum. Meth. A **506**, 250 (2003).
- [9] D. Brown, E. Charles and D. Roberts, “The *BABAR* Track Fitting Algorithm”, contributed paper to CHEP 2000.
- [10] The *BABAR* Collaboration, B. Aubert *et al.*, Phys. Rev. D **72**, 052006 (2005).
- [11] L. Lyons, D. Gibaut and P. Clifford, Nucl. Instrum. Meth. A **270**, 110 (1988).